ELSEVIER

Contents lists available at ScienceDirect

## Applied Catalysis A, General

journal homepage: www.elsevier.com/locate/apcata



# Rectifying the chemisorption – XRD discrepancy of carbon supported Pd: Residual chloride and/or carbon decoration



Ritubarna Banerjee, John R. Regalbuto\*

Department of Chemical Engineering, University of South Carolina, Columbia, SC 29208, United States

ARTICLE INFO

Keywords:
Carbon decoration
Palladium
Chemisorption discrepancy
STEM
XRD
Residual chloride

#### ABSTRACT

A conspicuous discrepancy is prevalent in the characterization of carbon supported palladium catalysts: particle size estimated by XRD and electron microscopy agree, while the chemisorption of hydrogen is substantially suppressed with respect to the small size measured by XRD/STEM. In this work, a systematic study of carbon materials, pretreatments, and characterization has isolated the contributions of carbon decoration and residual chloride, both of which can cause a chemisorption shortfall. The degree of decoration decreases with graphitization of the carbon supports due to stronger C—C interaction, whereas increased density of oxygen functional groups on the surface increases decoration, due to enhanced Pd-C interactions. The discrepancy can be rectified by employing a low temperature burnoff of the decorating carbon layers prior to chemisorption, and by using metal precursors without chloride ligands or counterions.

#### 1. Introduction

Carbon supported palladium catalysts are used in a wide variety of industrial processes including hydrogenation of alkenes, hydrogenation of aromatics, isomerization of hydrocarbons, oxidation of formic acid, hydrodechlorination, to name a few [1–5]. Typical heterogeneous catalysts in the industry consist of the transition metals deposited onto an inert support by a variety of deposition techniques. The deposition method is followed by drying/calcination and reduction to yield small metal nanoparticles for the purpose of maximizing the fraction of metal atoms exposed, given that reactants only access the surface of metal crystallites [6].

It is frequently seen in the literature in the characterization of palladium nanoparticles on carbon supports that the chemisorption of hydrogen is substantially suppressed on the catalysts leading to a disagreement between particle sizes obtained by STEM/XRD and chemisorption [7,8]. Krishnakutty and Vannice first observed this discrepancy for Pd dispersed on carbon black and attributed the suppression of hydrogen chemisorption to carbon contamination [9]. It was suggested that during the pre-treatment and synthesis, the C atoms could occupy both the bulk interstitial and surface sites of the Pd nanoparticles. While a carbon overlayer might be beneficial for increasing the hydrothermal stability of nanoparticles in a reaction environment [10], it can also reduce the activity and selectivity by blocking the active sites and poisoning the catalyst.

The chemisorption versus XRD/STEM discrepancy was recently studied in some detail in a series of carbon supported Pd catalysts where again, the discrepancy was more definitively attributed to the metal surface being coated with a partial or complete overlayer of carbon that blocked the active metallic sites for adsorption [7]. Temperature programmed oxidation (TPO) was employed to burn off the surface and sub-surface carbons and more fully expose the metallic surface. Although this discrepancy has been more commonly noticed in carbon supported palladium nanoparticles, it has also been seen in ruthenium nanoparticles supported on carbon [11].

Despite being observed with some frequency in the literature, the suppression of chemisorption in Pd/C catalysts is only now beginning to be understood, with an initial unambiguous demonstration of carbon decoration [7]. Expanding on that work, a systematic survey has been made to understand the effects of precursor ligands, pre-treatment, surface functionalization, and types of carbon supports on this discrepancy. The different carbons employed originate from different sources: carbon black, activated carbon and graphitic carbon. These are subjected to different pretreatment and oxidizing conditions to modify their surface functionalities and composition. By understanding the origin and mechanism of Pd site blockage, definitive means to avoid or eliminate it are prescribed.

E-mail address: regalbuj@cec.sc.edu (J.R. Regalbuto).

<sup>\*</sup> Corresponding author.

#### 2. Materials and methods

### 2.1. Materials and pretreatments

A carbon black (VXC72, Cabot Corporation), an activated carbon (DarcoG60, Sigma Aldrich) and a graphitic carbon (Timrex HSAG300, Timcal) were employed. Some of the VXC72 and DarcoG60 carbon was oxidized by boiling in nitric acid (> 70 %) at 90 °C for 3 h and cooling to room temperature. The mixture was filtered and washed with deionized (DI) water until the pH of the washing solutions reached that of DI water, and was subsequently dried overnight at room temperature. This was followed by annealing each of the oxidized and unoxidized carbons in argon to 300°C, 600°C and 1000°C for 16 h. The BET surface areas were determined from nitrogen adsorption-desorption isotherms with a Micromeritics 2020 ASAP instrument.

The point of zero charge (PZC) was determined by measuring the initial and final pH of a series of thick slurries at high surface loadings which generally gives a wide plateau over which the final pH remains constant even as the initial pH changes [12,13]. This constant pH reflects the PZC of the supports. Based on the PZC of the support, cationic or anionic Pd precursors were chosen for performing strong electrostatic adsorption (SEA). For the low PZC oxidized VXC72, oxidized DarcoG60 and Timrex carbons, the cationic precursor, tetraamminepalladium(II) chloride (PdTA, (Pd(NH<sub>3</sub>)<sub>4</sub>)Cl<sub>2</sub>, Sima-Aldrich 99.999 %) was used. For the high PZC unoxidized VXC72 and DarcoG60, palladium(II) chloride, PdCl2 (Sigma-Aldrich 99.9 %) was stabilized with excess HCl, forming palladium tetrachloride, PdTC, (PdCl<sub>4</sub>)<sup>2-</sup>, and this was used as the anionic precursor. A 5.6:1 ratio of PdCl<sub>2</sub>:HCl was used based on the literature [14]. Table 1 shows the pretreatment for the two types of carbon along with the corresponding PZCs and precursors used.

## 2.2. Adsorption surveys and supported nanoparticle preparation

Strong electrostatic adsorption [15–17] was used to prepare the supported nanoparticles. Adsorption surveys were conducted for all the series of oxidized, heat treated samples after the precursors were chosen based on the PZC. Solutions over an entire range of pH (1–13) were prepared at constant concentration (200 ppm). The high PZC unoxidized supports were weighed out to obtain a 500 m $^2$ /L surface loading and the low PZC oxidized supports, weighed out for 1000 m $^2$ /L, were added to the solutions and shaken vigorously for about an hour. The solutions were then filtered and initial and final concentrations were determined in an ICP-OES. The uptake of palladium was calculated from the difference in the concentration. Once the optimal pH of

Table 1
Pre-treatment, PZCs and surface areas of VXC72, DarcoG60 and Timrex.

Support	Pre-Treatment Temperatures (°C)	Oxidized	PZC	Precursor	
VXC72	0	No	8.2	PdTC	
	300		8.3		
	600		8.3		
	1000		10		
	0	Yes	2.3	PdTA	
	300		2.3		
	600		2.3		
	1000		2.5		
DarcoG60	0	No	8.1	PdTC	
	300		9.1		
	600		10.2		
	1000		11.1		
	0	Yes	1.7	PdTA	
	300		2.8		
	600		3.2		
	1000		3.8		
Timrex	0	No	4.1	PdTA	

adsorption was determined, the supported Pd nanoparticles were prepared with a metal loading of 2.5 wt% for the unoxidized VXC72 and a weight loading of 10-11 wt% for the unoxidized and oxidized Darco. This was followed by oven drying in static air at 120 °C for 16 h and then, reduction at 150-180 °C in flowing 10 %  $\rm H_2$  balance He for 1 h as determined from temperature programmed reduction with a ramp rate of 2.5 °C/min.

### 2.3. Catalyst characterization

The supported nanoparticles were characterized using x-ray diffraction (XRD), scanning transmission electron microscopy (STEM) and chemisorption. A Rigaku Miniflex-II equipped with a high sensitivity D/teX Ultra silicon strip detector was used to perform powder XRD on the supported Pt particles. Patterns were recorded over a range of  $10^\circ\text{--}80^\circ$  20 using Cu-K $\alpha$  radiation (k = 1.5406 Å) at 30 mA and 15 kV [18]. XRD patterns were obtained for all metal free supports in addition to the supported metals. Background subtraction and deconvolution of peaks contributed by Pd and carbon support were done in PDXL 2.0 provided by Rigaku, using the Split Pseudo-Voigt function for the peaks. The full width at half maximum (FWHM) values were input together with a shape factor of 0.94 in the Scherrer equation to estimate particle size.

An aberration-corrected JEOL 2100 F scanning transmission electron microscopy (STEM) was used to do Z-contrast imaging with a 200 kV field emission gun and a double tilt holder for tilting the sample across a range of angles ( $\pm$ 20°). Sample preparation involved ultrasonicating the sample in ethanol and adding a drop to a copper TEM grid with a thin holey carbon coating. High angle annular dark-field (HAADF) STEM images were acquired on a Fischione Model 3000 HAADF detector with a camera length such that the inner cut-off angle of the detector was 50 mrad [19]. The images were recorded using Digital Micrograph software and particle size distributions were obtained by counting about 1000 particles on each sample. The number average diameter  $D_n = \Sigma n_i d_i^{\ 2}/\Sigma n_i d_i$ , the surface average diameter  $D_s = \Sigma n_i d_i^{\ 3}/\Sigma n_i d_i^{\ 2}$  and the volume average diameter  $D_v = \Sigma n_i d_i^{\ 4}/\Sigma n_i d_i^{\ 3}$  were calculated where  $n_i$  is the number of particles with diameter  $d_i$  [201.

Pulse chemisorption of the samples was performed using a Micromeritics Autochem 2020 instrument. The process involved hydrogen titration of oxygen pre-covered Pd surfaces. A pretreatment step included drying at 120°C followed by reduction in 10 % hydrogen at 200°C. The catalyst was then contacted with 10 % oxygen in helium at 40°C for 30 min to oxidize the surface Pd to PdO. Then, it was titrated with pulsed 10 % hydrogen in argon to form water and chemisorbed hydrogen. The assumed overall stoichiometry is 0.667 Pd:1 H<sub>2</sub>. This procedure and stoichiometry have been thoroughly demonstrated for Pd catalysts in previous work [21]. Particle sizes were estimated from chemisorption assuming hemispherical geometry. Since chemisorption is a surface technique, it is compared to surface average STEM sizes and XRD, being a volume/bulk technique is compared to the volume average STEM sizes [20].

A series of catalyst samples were prepared by introducing an additional oxidation step in the chemisorption protocol for burning off the surface carbon on the palladium metal nanoparticles. In this step, the catalysts were heated to a temperature of  $300^{\circ}$ C in 10~% oxygen and balance helium at 20~sccm followed by the standard reduction and chemisorption protocol [7].

## 3. Results and discussion

## 3.1. Adsorption surveys

It has been previously established in the literature that the PZC of carbon surfaces can be irreversibly altered by oxidation, thereby giving the flexibility of adsorbing either a cation or anion based on the PZC [15,16]. As observed from Table 2, both the process of surface

**Table 2**Particle size from XRD, Chemisorption and STEM for VXC72 and DarcoG60.

Carbon Type	Pretreatment Temperature (°C)	XRD Sizes (nm)	STEM Volume Average Sizes, Dv (nm)	Pre-Burnoff Chemisorption Sizes (nm)	Post-Burnoff Chemisorption Size (nm)	STEM Surface Average Sizes, Ds (nm)
Un-oxidized VXC72	_	2.4	1.5 ± 0.4	3.3	3.5	1.5 ± 0.4
	300	2.5	$1.8 \pm 0.4$	3.5	2.4	$1.7 \pm 0.4$
	600	2.9	$2.7 \pm 0.9$	3.6	2.1	$2.4 \pm 0.8$
	1000	3	$4.4 \pm 2.7$	3.9	3.1	$3.1 \pm 1.5$
Oxidized VXC72	_	< 1.5	1.5 ± 0.4	6.3	3.8	$1.4 \pm 0.4$
	300	< 1.5	$1.6 \pm 0.4$	6.4	3.1	$1.5 \pm 0.4$
	600	< 1.5	$1.6 \pm 0.3$	6.4	2.4	$1.6 \pm 0.3$
	1000	< 1.5	$1.9 \pm 0.5$	6.5	2.7	$1.8 \pm 0.5$
Un-oxidized Darco	_	12.5	11.7 ± 8.9	8.1	7.2	7.7 ± 5.2
G60	300	13.8	$13.1 \pm 10.1$	8.6	7.3	$8.6 \pm 5.8$
	600	14.7	14.9 ± 11.9	11.4	10.9	$10.6 \pm 7.9$
	1000	17.5	$16.9 \pm 15.0$	12.6	11.1	$11.6 \pm 9.7$
Oxidized Darco G60	_	< 1.5	$1.8 \pm 0.6$	3.2	1.4	1.7 ± 0.5
	300	< 1.5	$1.9 \pm 0.7$	3.5	2	$1.8 \pm 0.6$
	600	< 1.5	$2.0 \pm 0.7$	3.9	2.2	$1.9 \pm 0.6$
	1000	< 1.5	$2.3 \pm 0.7$	4.1	2.6	$2.2 \pm 0.6$
Timrex	_	< 1.5	$1.6 \pm 0.4$	2.1	1.4	$1.6 \pm 0.3$

oxidation as well as annealing the carbons at various temperatures alters the PZC. While surface oxidation for both the VXC72 and the DarcoG60 decreases the PZC, heating the carbons increases it. Once PZC of the support was determined, a precursor was chosen and uptake experiments were performed to determine the maximum adsorption pH.

A summary of metal uptake versus pH for the four sets of carbons is shown in Fig. 1. As expected, the uptake for all the carbons using SEA was volcanic in shape: the uptake increases as the pH moved further away from the PZC but decreases at high pH due to high ionic strength. The color codes in the plots designate the pretreatment temperatures.

For both the oxidized and unoxidized VXC72 (Fig. 1a and b), the uptake of palladium is in the range of 1.2–1.4  $\mu\text{-moles/m}^2$  which translates to metal loadings of 2.5 wt% while for the DarcoG60 oxidized and unoxidized carbons (Fig. 1c and d), the uptake is in the range of 1.5–1.7  $\mu\text{-moles/m}^2$  which translates to metal loadings of about 11 wt%. At the same surface density, the difference in the weight loadings for the two carbons is due to the difference in their surface area: VXC72 has a surface area of 250 m²/gm while that of Darco is 650 m²/gm. In each sample set, the small variation in PZC caused by annealing has a noticeable effect on the uptake and follows expected trends as established by the Revised Physical Adsorption (RPA) model [22]. From the

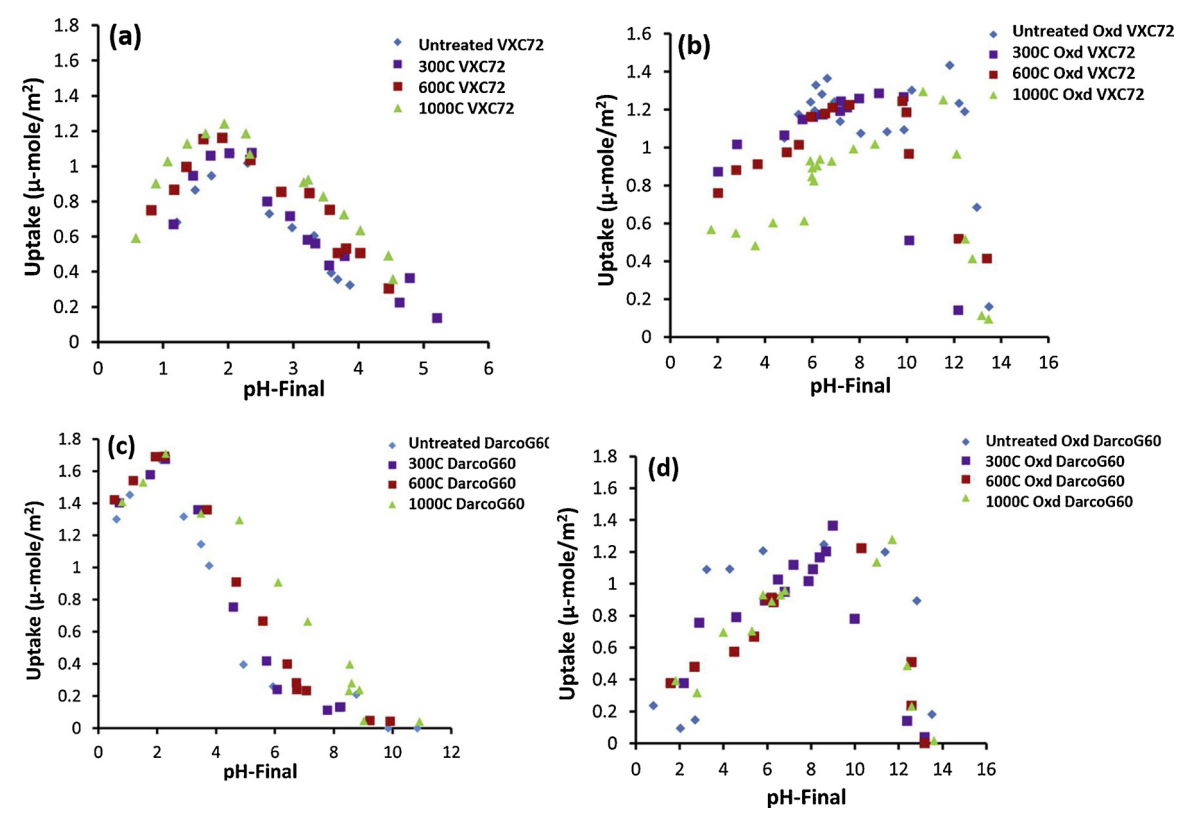


Fig. 1. Uptake Plots (a) Unoxidized VXC72 (b) Oxidized VXC72 (c) Unoxidized DarcoG60 (d) Oxidized DarcoG60.

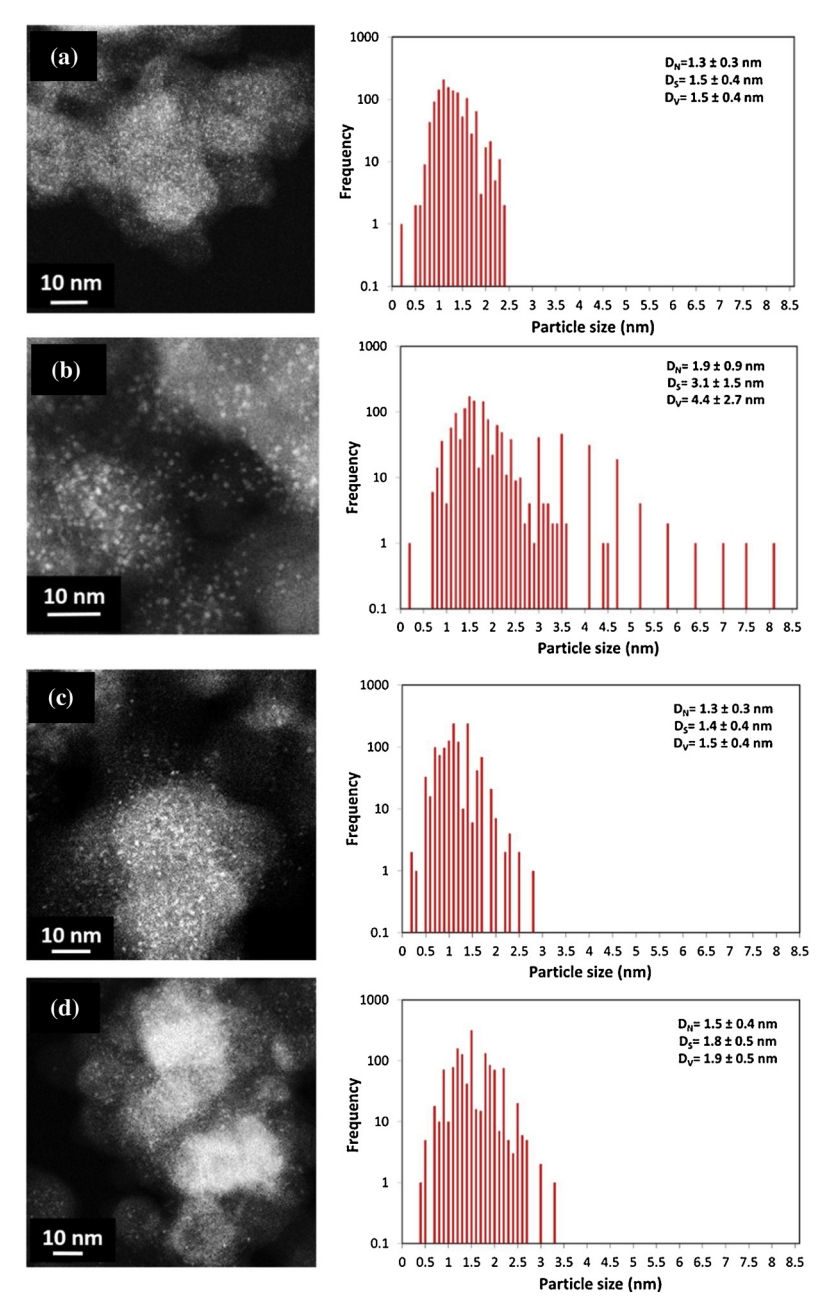


Fig. 2. STEM images for (a) unoxidized VXC72 (b) unoxidized VXC72 annealed to 1000 °C (c) oxidized VXC72 (d) oxidized VXC72 annealed to 1000 °C (e) unoxidized DarcoG60 (f) unoxidized DarcoG60 annealed to 1000 °C (g) oxidized DarcoG60 (h) oxidized DarcoG60 annealed to 1000 °C (i) TimrexHSAG.

untreated to the 1000°C annealed VXC72 and DarcoG60 (Fig. 1a and c), the PZC increases resulting in higher uptakes for PdTC. The 1000°C annealed VXC72 and DarcoG60 absorb the highest amount of PdHC. For the oxidized carbons (Fig. 1b and d), as the annealing temperature of the carbons is increased, the PZC increases but this results in lower uptakes of the PdTA cationic precursor.

Once the optimal pH of adsorption was determined, the supported Pd nanoparticles were prepared with a metal loading of 2.5 wt% for the unoxidized VXC72 and a weight loading of 11 wt% for the unoxidized and oxidized Darco. This was followed by drying at 110 °C overnight and reduction at 150-180 °C in 10 % flowing hydrogen to yield the metal nanoparticles. The reduction temperatures were determined by Temperature Programmed Reduction (TPR) experiments on each series of carbon.

Fig. 2 shows representative STEM images for the VXC72 and DarcoG60 carbons along with their particle size histograms. Only the

untreated and 1000°C treated carbon supports are shown in the figure. Images and histograms of the other two series heat treated at 300°C and 600°C are included in the supporting information (Figures S1-S4). In Table 2, volume and surface average particle sizes from the STEM histograms of all samples are summarized (for comparison with XRD and chemisorption measurements respectively). Over the unannealed VXC72 carbon black support (Fig. 2a and c), SEA with either precursor gives rise to 1.5 nm volume averaged particle size. The volume average size grows to 4.4 nm for the annealed, unoxidized VXC72 support/ chloride precursor (Fig. 2b), and to 1.9 nm for the annealed, oxidized VXC72 support/ammine precursor (Fig. 2d). The volume average particle size starts large (11.7 nm) for the unoxidized DarcoG60 activated carbon support/chloride precursor (Fig. 2e) and grows to 16.9 nm for the highest annealing temperature (Fig. 2f), while the size of the oxidized DarcoG60 support/ammine precursor (Fig. 2g) starts small (1.8 nm) and grows to 2.3 nm for the highest annealing temperature

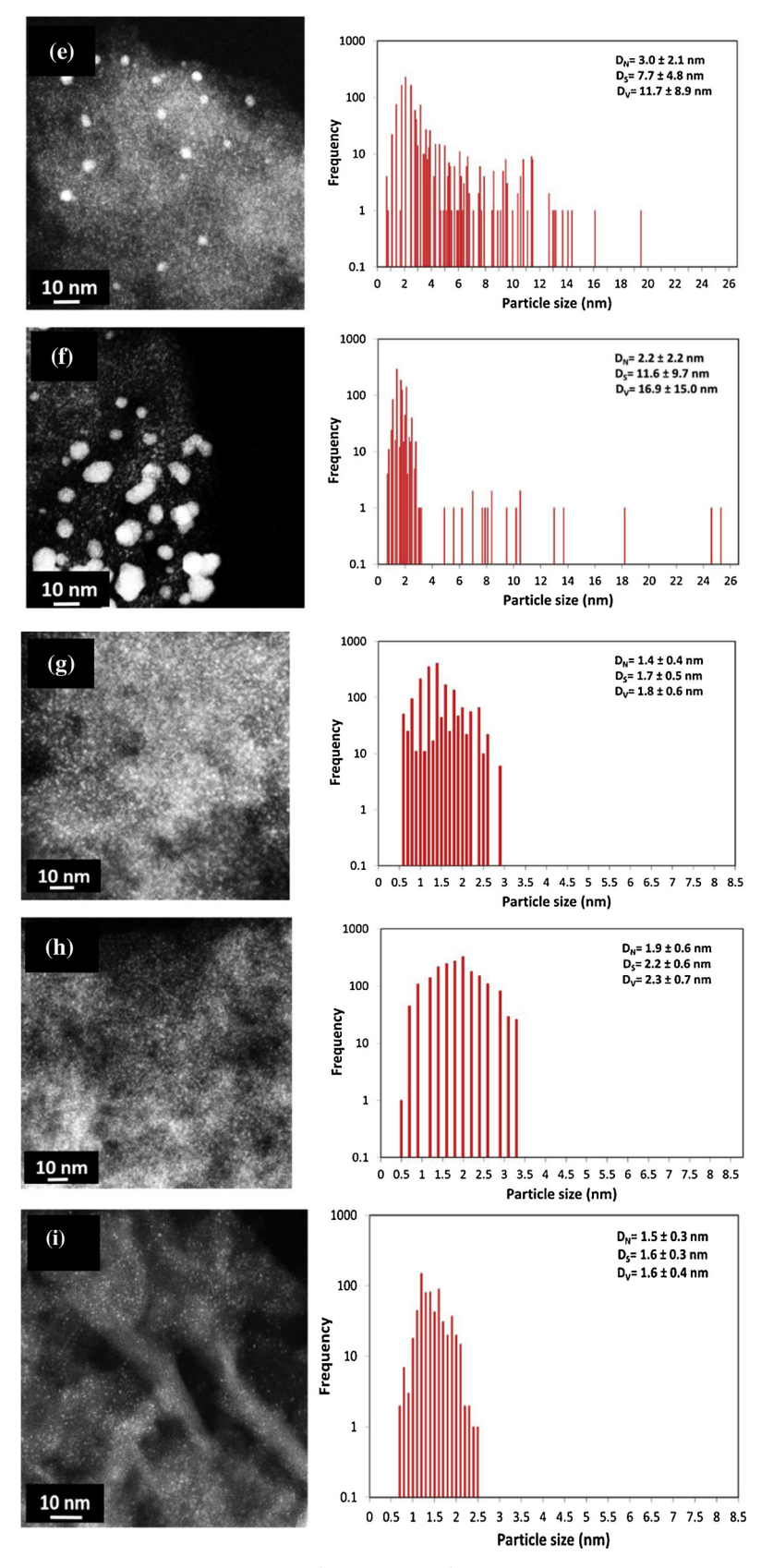


Fig. 2. (continued)

(Fig. 2h). The unannealed graphitic carbon Timrex sample/ammine precursor (Fig. 2i) yields a volume average particle size of 1.6 nm. The increase in average particle sizes with increasing support pretreatment temperature is likely due to the removal of oxygen functional groups on

the support on annealing, as indicated by the increased PZC values. Oxygen functional groups on carbon have been cited to anchor crystallites of Pd and Pt and increase metal dispersion [23–26].

Fig. 3 contains XRD patterns corresponding to the samples seen in

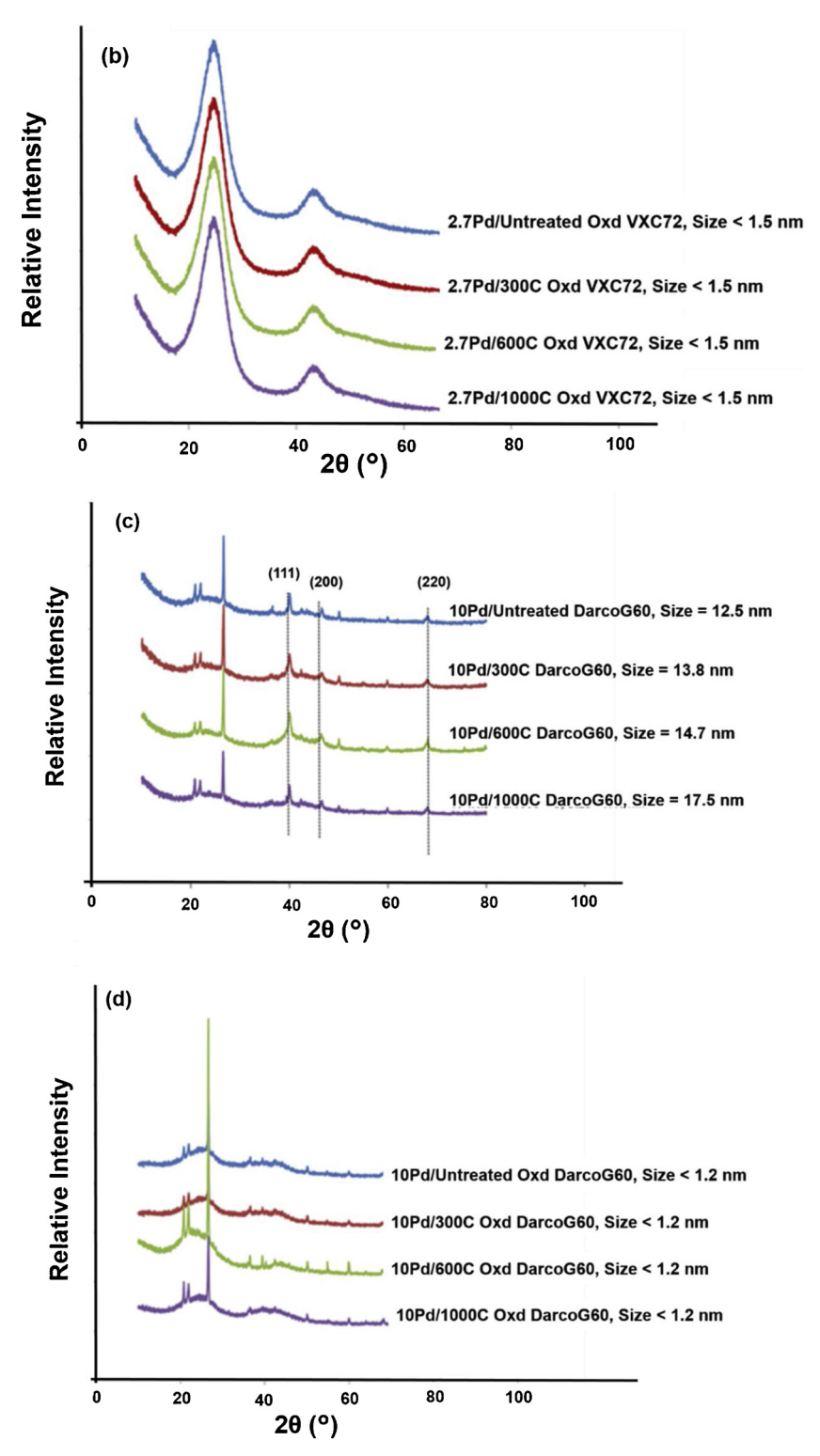


Fig. 3. XRD patterns for (a) unoxidized VXC72 (b) oxidized VXC72 (c) unoxidized Darco and (d) oxidized Darco.

Fig. 2. For the oxidized carbons, the particles are too small to be seen by XRD. The absence of XRD patterns for those samples with STEM volume averages above 1.5 nm can be explained by the relatively low mass fraction of particles of these samples being in the detectable range.

Nanoparticles are observable by XRD for the unoxidized black and activated carbon, and the XRD estimates of size, given in Table 2, agree reasonably well for the VXC72 samples, and very well for the DarcoG60 samples, and confirm the increase in size with increased support annealing temperature. Unexpectedly in view of the behavior of Pt [11],

the entire series of unoxidized Darco gave large Pd particles with wide standard deviations. Both XRD and STEM confirmed that large particles with wide standard deviations were obtained for the unoxidized Darco (Figs. 2e, f and 3 c). However, if the support is oxidized, the particle size is small (Figs. 2g, f and 3 d). A hypothesis to explain the large particle sizes of the unoxidized DarcoG60 is the phenomenon of deposition precipitation at the surface of the support. It has been seen in the literature [22,27] that although the global pH of the solution may be regulated, the local pH in the vicinity of a surface may increase due to

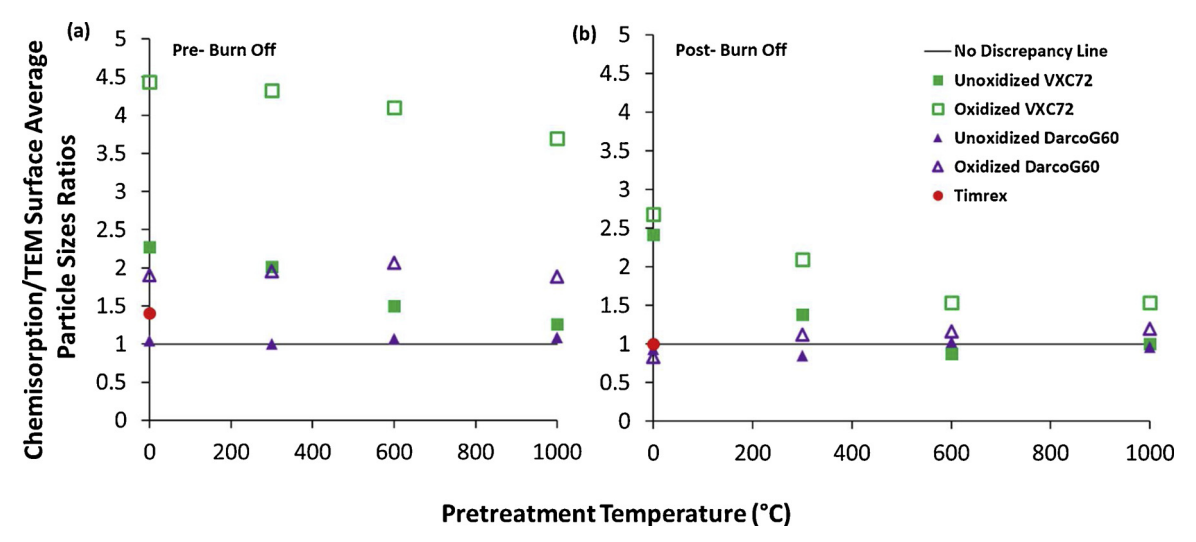


Fig. 4. Chemisorption/STEM particle size discrepancy with annealing temperature, for chemisorption measurements made a) without and b) with a preliminary burn-off procedure.

interactions between the complex precursor ion species (in this case,  $PdCl_4^{2-}$ ) leading to a protonation of the support surface. This local pH increase may cause the Pd complex, which is less robust than the corresponding Pt complex [15] to precipitate on the support leading to larger particles. (A greater amount of HCl may be required to stabilize the PdTC complex in solution, though this was not tested.)

Chemisorption results are summarized in Table 2 and compared to the XRD and STEM size estimates. Each series shows a decrease in chemisorption uptake and corresponding increase in chemisorption-estimated particle size with increasing annealing temperature. This is consistent with the XRD and STEM trends. For the case of the unoxidized DarcoG60 support there is excellent agreement between XRD and STEM volume-average size estimates, as well as between chemisorption and STEM area-averaged size estimates. For all other series, the chemisorption size estimates are considerably higher than the STEM/XRD sizes.

This discrepancy is plotted as the ratio of chemisorption-derived size to STEM surface average sizes versus the pre-treatment temperatures in Fig. 4a. The horizontal line at the chemisorption/STEM ratio of 1 depicts agreement of the estimates. It is observed that the discrepancy for both the VXC72 and DarcoG60 carbons is the highest when they are oxidized. It is also seen that increase in pretreatment temperature for each of the oxidized and unoxidized series decreases the discrepancy. The latter observation agrees well with the former in that the amount of oxygen groups on the surface decreases with increases in annealing temperatures and hence, the lesser oxidized carbons show lower discrepancy. The reason behind the greater discrepancy exhibited by oxidized carbons may be attributed to the lone pair of electrons around the C=O bonds (in carboxylic acid or anhydride groups) that are shared with the 4d orbitals of the Pd leading to strong Pd-C interaction which enhances carbon decoration. This strong interaction between the Pd nanoparticles and the oxidized carbons has been explained as the main reason for the formation of a carbon shell coated on Pd nanoparticles which could prevent agglomeration of the Pd nanoparticles during heating [28,29].

An additional observation is that the unoxidized Darco which gave large particles did not show a discrepancy. This may be due to the higher activation energy required for diffusion of carbon atoms onto the surface of large palladium nanoparticles as compared to smaller ones. It was also observed that the degree of discrepancy was higher for VXC72, a carbon black, than the DarcoG60, an activated carbon. It should also be noted here that the graphitic carbon, TimrexHSAG did not show any significant decoration: the ratio of Chemisorption to STEM sizes diminished from 1.5 to 1.0 after the burnoff. The degree of graphitization

of the carbon support on the degree of discrepancy will be discussed in detail later.

In previous work [7] it was demonstrated that decorating carbon could be burned off in oxygen at a moderate temperature, that is, substantially below the temperature at which the carbon combusted. A pre-oxidation step (20 sccm  $10~\%~O_2$  in He at  $300~^\circ$ C) was thus added to the chemisorption measurement for the purpose of removing any decorating carbon. These results are summarized in Table 2 and are plotted versus annealing temperature in Fig. 4b. The burnoff had no appreciable effect on the unoxidized DarcoG60 series, which had no discrepancy to begin with, but it did bring the oxidized DarcoG60 series and the Timrex sample into agreement. The burnoff also substantially lowered the discrepancy of the oxidized and unoxidized VXC72 series.

A comparison of Fig. 4a and b shows that although the discrepancy reduced after the burnoff, it is not entirely eliminated. It almost disappeared for the oxidized Darco but was still significant for the oxidized VXC72. Thus burning off the surface carbon does not in general recover the chemisorption surface completely. The other possible mechanism is chloride poisoning of the Pd surface.

To examine this mechanism, three different carbons were selected: oxidized VXC72 (carbon black), oxidized DarcoG60 (activated carbon) and TimrexHSAG300 (graphitic carbon). The Pd salt (NH<sub>3</sub>)<sub>4</sub>PdCl<sub>2</sub> (PdTA with Cl<sup>-</sup> counterion) was compared with (NH<sub>3</sub>)<sub>4</sub>Pd(NO<sub>3</sub>)<sub>2</sub> (PdTA with NO<sup>3-</sup> counterion). There was no noticeable differences in the STEM surface average sizes between using the two different precursors on any of the three supports, as shown in Fig. 5.

Fig. 6 is a plot of the chemisorption/STEM ratio for the different types of carbons comparing the nitrate vs the chloride precursors. For each of the carbons, comparing the pre-TPO chemisorption/STEM ratio shows 20-50 % decrease in the discrepancy when using a nitrate precursor as compared to using a chloride precursor. For the chloride precursors used earlier, it was seen earlier for the oxidized VXC72 and DarcoG60 that the TPO treatment gave a 50 % decrease in the discrepancy. This was also seen for the Timrex support where the discrepancies reduced after the carbon burnoff for the chloride precursors. Hence, using a non-chloride precursor coupled with carbon burnoff treatments should ideally recover the entire surface on all the carbon supports. This was found to be true as shown in Fig. 6 for the carbon supports when comparing the post TPO ratio with the nitrate precursors. Although SEA should ideally filter away the chloride anions, it appears that some residual chloride still remains on the metal and/or carbon, post filtration, and after reduction this ends up poisoning the surface. There has been mention in the literature of Cl ions issued during the decomposition of platinum (IV) hexachloride or Pt (II)

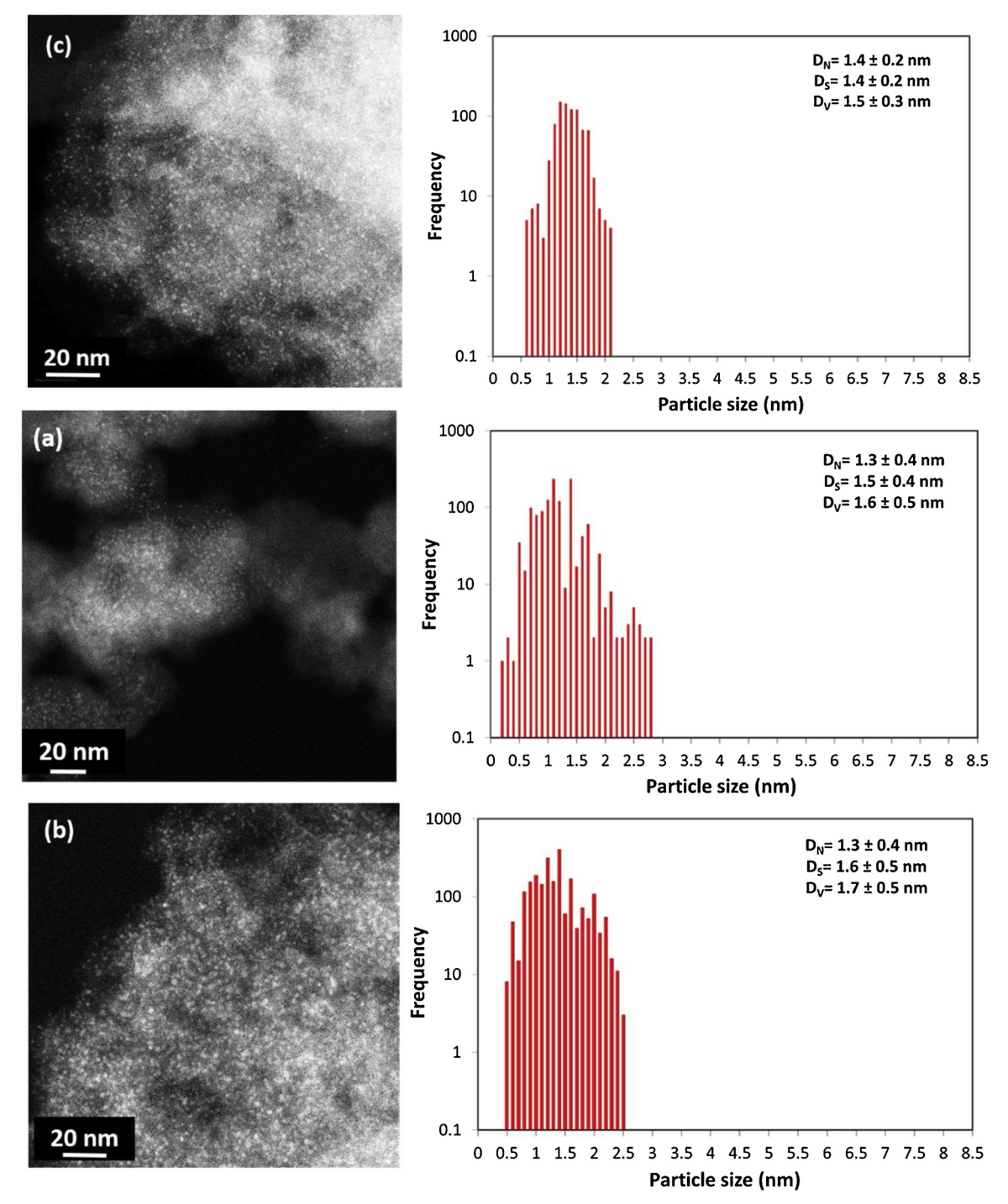


Fig. 5. STEM images for (a) Pd on oxidized VXC72 (b) Pd on oxidized DarcoG6 and (c) Pd on TimrexHSAG300 using nitrate precursors.

tetrachloride precursors partially blocking Pt catalytic sites [30,31]. Prolonged, high reduction temperatures may remove the chloride from the metal surface, at a risk of sintering the particles. The simplest solution, if possible, is to avoid the use of chloride as the balancing ion in precursors, using nitrate or hydroxide salts instead.

The dependence of the discrepancy on the degree of graphitization can be analyzed by the XRD data in Fig. 7. The order of support graphitization is oxidized VXC72 (no graphitization) < oxidized Darco < Timrex. The degree of discrepancy corresponds inversely to the degree of graphitization.

The decrease in the interlayer spacing which accompanies increasing graphitization has long been established in the literature [32–35]. Graphitic carbons have a layered structure with an interlayer

spacing of 3.35A and in each layer, a carbon atom is bonded to 3 neighbors at 1.42Á, forming a two dimensional hexagonal net. Additionally, half of the atoms in a layer are directly over atoms in the previous layer, and the other half are over the centers of the hexagons [33]. It is suggested that increased graphitic content causes an enhanced C—C interaction due to the long range ordering of the graphitic basal planes which is stronger relative to Pd-C interactions. Thus oxidized VXC72, a carbon black with no graphitization and high number of oxygen groups has the strongest Pd-C interaction and the highest degree of carbon decoration. Oxidized Darco, an activated carbon with partial graphitization and high number of oxygen groups present, displays an intermediate degree of carbon decoration. Timrex, a graphitic carbon with very few oxygen groups, has C—C interaction much stronger than

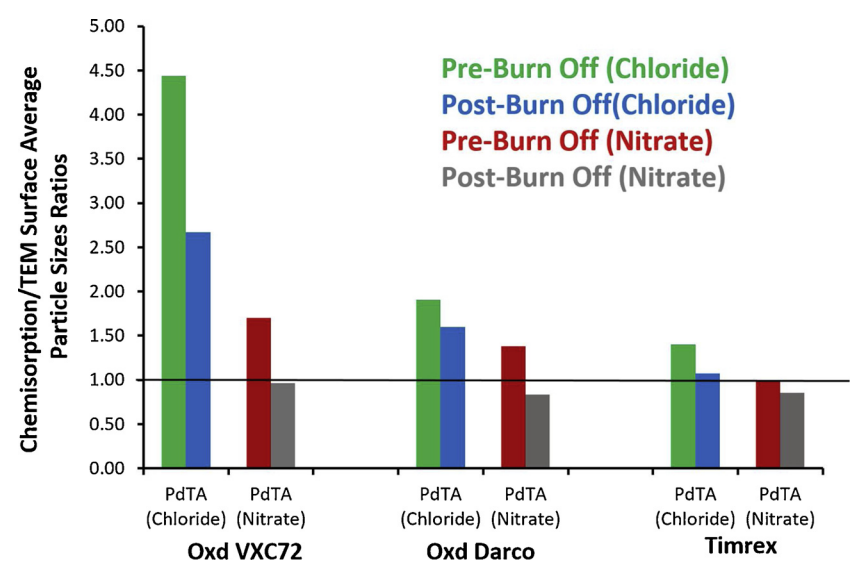


Fig. 6. Chemisorption particle size comparison using nitrate vs chloride ions for oxidized VXC72, oxidized Darco and Timrex.

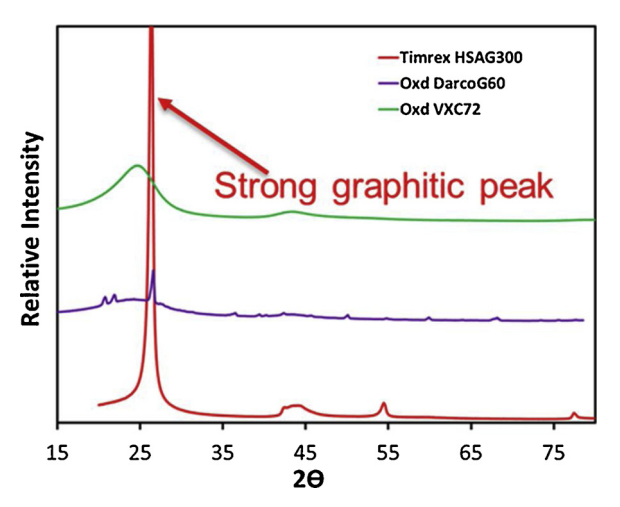


Fig. 7. XRD of the carbon supports showing degree of graphitization.

Pd-C interaction due to long range ordering and absence of oxygen groups and so displays the lowest degree of carbon decoration.

Fig. 8 summarizes the proposed causes of the chemisorption-estimated particle size discrepancy: carbon decoration and/or chloride

contamination. The decomposition of the precursor may be initiated during drying and hence, chloride contamination may happen both during drying and reduction. There are mixed opinions in the literature of the stage at which carbon decoration occurs. While Krishnakutty and Vannice [9] claim that the reduction process is responsible for the carbon decoration, Tengco et al. [7] have shown that once the overlayers have been removed by burnoff, they do not reform after additional reductions. It would thus appear that the origin of the overlayers is at the onset of nanoparticle formation from the adsorbed precursors; at this stage the Pd atoms would be in closest proximity to the carbon surface. Their formation at this early stage can explain the observation in the prior work that the degree of discrepancy was highly sensitive to the pretreatment of the adsorbed precursors [7]. Higher discrepancies were seen for a reduced precursor than one annealed in an inert, and higher still was the discrepancy and the amount of decorating carbon of a calcined precursor. The reactive pretreatments are hypothesized to more quickly remove the metal ligands of the precursor and so permit stronger Pd-C interactions during nanoparticle formation. This notion is also consistent with the lack of decoration of the largest particles (unoxidized Darco G60 in Figs. 2f and 3 c); in the case that nanoparticles nucleate and grow large quickly, the Pd-C interaction is diminished.

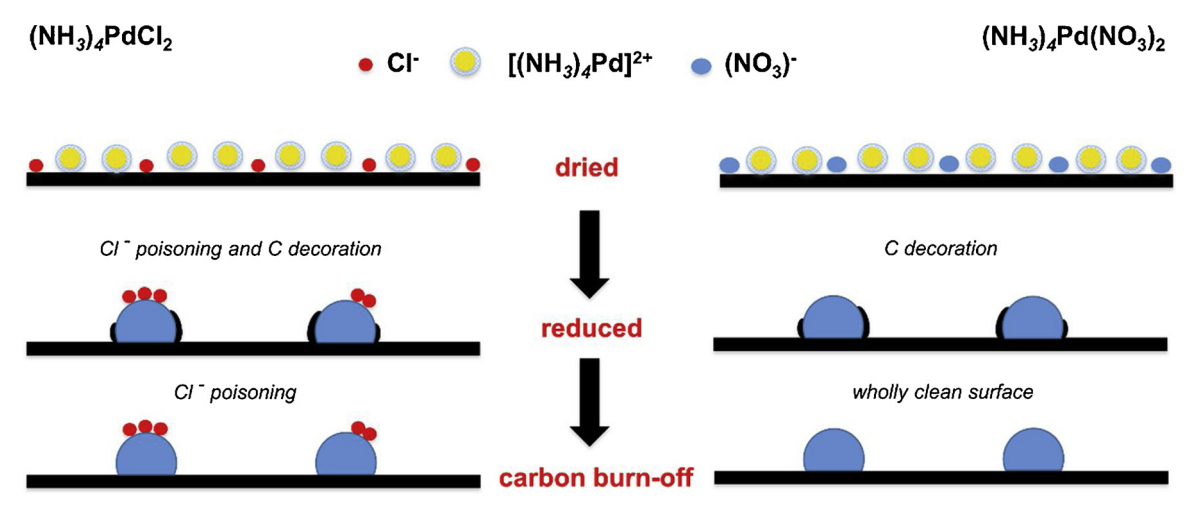


Fig. 8. Schematic illustration of carbon decoration and chloride poisoning in carbon supported palladium nanoparticles.

#### 4. Conclusions

A systematic study was performed to understand the effect of carbon supports, surface functional groups, heat treatments and precursors on the discrepancy in particle size estimated by chemisorption versus STEM or XRD (the latter two of which agree). While the degree of discrepancy decreased with graphitization of the carbon supports due to stronger C–C interaction, increase in oxygen functional groups on the surface increased the discrepancy due to enhanced Pd-C surface interactions. TPO was able to recover only about 50 % of the metal surface and the remaining portion is attributed to chloride contamination which could be avoided by using nitrate or any other non-chloride precursor. Hence, the steps for avoiding the discrepancy involves utilizing non-chloride precursors and introducing a carbon burnoff step prior to chemisorption.

#### **Author contributions**

The manuscript was written through contributions of all authors. All authors have given approval to the final version of the manuscript.

### Acknowledgments

The authors would like to acknowledge Dr. Doug Blom for special assistance with electron microscopy in this work, as well as partial support from NSF grant IIP 1464630 and the South Carolina Smartstate Center of Catalysis for Renewable Fuels.

## Appendix A. Supplementary data

Supplementary material related to this article can be found, in the online version, at doi:https://doi.org/10.1016/j.apcata.2020.117504.

#### References

- [1] S.D. Jackson, L.A. Shaw, Appl. Catal., A: Gen. 134 (1996) 91-99.
- [2] H.U. Blaser, A. Indolese, A. Schnyder, H. Steiner, M. Studer, J. Mol. Catal. A Chem. 173 (2003) 3–18.
- [3] L. Yin, J. Liebscher, Chem. Rev. 107 (2007) 133-173.

- [4] D. Morales-Acosta, J. Ledesma-Garcia, L.A. Godinez, H.G. Rodriguez, L. Alvarez-Contreras, L.G. Arriaga, J. Power Sources 195 (2010) 461–465.
- [5] A.L.D. Ramos, P. da Silva Alves, D.A.G. Aranda, M. Schmal, Appl. Catal., A: General 277 (2004) 71–81.
- [6] J.W. Niemantsverdriet, Spectroscopy in Catalysis: An Introduction, 3rd edition, Wiley-VCH Verlag GmbH & Co. KGaA, Weinheim, Germany, 2007 p 297.
- [7] J.M.M. Tengco, Y.K.L. Jose, J.R. Monnier, Catal. Today 246 (2015) 9-14.
- [8] C. Amorim, M.A. Keane, J. Colloid Interface Sci. 322 (2008) 196-208.
- [9] N. Krishnakutty, M.A. Vannice, J. Catal. 155 (1995) 312–326.
- [10] H.N. Pham, A.E. Anderson, R.L. Johnson, T.J. Schwartz, B.J. O'Neill, P. Duan, K. Schmidt-Rohr, J.A. Dumesic, A.K. Datye, ACS Catal. 5 (2015) 4546–4555.
- [11] S. Cao, Rational Synthesis to Optimize Ruthenium-Based Biomass Conversion Catalysts, Ph.D. Dissertation University of South Carolina, Columbia, 2016.
- [12] J.R. Regalbuto, J. Regalbuto (Ed.), Catalyst Preparation: Science and Engineering, Taylor and Francis, Boca Raton, FL, 2007p 297.
- [13] J. Park, J.R. Regalbuto, J. Colloid Interface Sci. 175 (1995) 239-252.
- [14] N. Santhanam, T.A. Conforti, W. Spieker, J.R. Regalbuto, Catal. Today 21 (1994) 141–156.
- [15] J.R. Regalbuto, K. de Jong (Ed.), Synthesis of Solid Catalysts, Chapter 3: Electrostatic Adsorption, Wiley-VCH Verlag, 2009.
- [16] L. D'Souza, J.R. Regalbuto, J.T. Miller, J. Catal. 254 (2008) 157–169.
- [17] X. Hao, S. Barnes, J.R. Regalbuto, J. Catal. 279 (2011) 48-65.
- [18] K. O'Connell, J.R. Regalbuto, Catal. Lett. 145 (2015) 777-783.
- [19] H.R. Cho, J.R. Regalbuto, Catal. Today 246 (2015) 143-153.
- [20] A.K. Datye, Q. Xu, K.C. Kharas, J.M.M. McCarty, Catal. Today 111 (2006) 59-67.
- [21] S. Riyapan, Y. Zhang, A. Wongkaew, B. Pongthawornasakun, J.R. Monnier, J. Panpronot, Catal. Sci Tech. 6 (2016) 5608–5617.
- [22] J.R. Regalbuto, R. Richards (Ed.), Surface and Nanomolecular Catalysis, CRC Press, 2006p 161.
- [23] D.J. Suh, P. Tae-Jin, I. Son-Ki, Carbon 31 (1993) 427-435.
- [24] V.Z. Radkevich, T.L. Senko, K. Wilson, L.M. Grishenko, A.N. Zaderko, V.Y. Diyuk, Appl. Catal., A: Gen. 335 (2008) 241–251.
- [25] C. Li, Z. Shao, M. Pang, C.T. Williams, C. Liang, Catal. Today 186 (2012) 69–75.
- [26] C. Alegre, M.E. Gálvez, E. Baquedano, E. Pastor, R. Moliner, M.J. Lázaroa, Int. J. Hydrogen Energy 37 (2012) 7180–7191.
- [27] K.P. De Jong, Synthesis of Solid Catalysts, Wiley-VCH Verlag GmbH & Co. KGaA, Weinheim, 2009 p 111.
- [28] B. Zhang, D.S. Su, ChemCatChem 7 (2015) 3639-3645.
- [29] B. Zhang, L. Shao, W. Zhang, X. Sun, X. Pan, D.S. Su, ChemCatChem 6 (2014) 2607–2612.
- [30] N. Job, M. Chatenet, S. Berthon-Fabry, S. Hermans, F. Maillard, J. Power Sources 240 (2013) 294–330.
- [31] S. Lambert, N. Job, L. D'Souza, M.F.R. Pereira, R. Pirard, B. Heinrichs, J.L. Figueiredo, J.P. Pirard, J.R. Regalbuto, J. Catal. 261 (2009) 23–33.
- [32] B.P. Richards, J. Appl. Crystallogr. 1 (1968) 35-48.
- [33] B.E. Warren, J. Chem. Phys. 2 (1934) 551-555.
- [34] B.E. Warren, Phys. Rev. 59 (1941) 693-698.
- [35] J. Biscoe, B.E. Warren, J. Appl. Phys. 13 (1942) 364-371.